

Single Charge-Exchange Reactions and the Neutron Density at the Surface of the Nucleus

Bui Minh Loc,^{1,2} Naftali Auerbach,¹ and Dao T. Khoa³

¹*School of Physics and Astronomy,
Tel Aviv University, Tel Aviv 69978, Israel.*

²*Department of Physics, Ho Chi Minh City University of Pedagogy,
280 An Duong Vuong Street, District 5, Ho Chi Minh City, Vietnam.*

³*Institute for Nuclear Science and Technology,
VINATOM 179 Hoang Quoc Viet Rd., Hanoi, Vietnam.*

(Dated: July 23, 2018)

Abstract

In this work we study the charge-exchange reaction to Isobaric Analog State using two types of transition densities. We show that for projectiles that do not probe the interior of the nucleus but mostly the surface of this nucleus, distinct differences in the cross-section arise when the two types of transition densities are employed. We demonstrate this by considering the ($^3\text{He},t$) reaction.

I. INTRODUCTION

Single Charge-Exchange (SCX) reactions were and are now an excellent source of information about isovector properties of nuclei. In particular successful is the SCX to the isobaric analog state (IAS). In this process one is able to probe the distribution of the isovector nuclear density. The IAS is defined as:

$$|A\rangle = \frac{1}{\sqrt{2T}} T_- |\pi\rangle, \quad (1)$$

where $|A\rangle$ denotes the IAS, $|\pi\rangle$ the parent state with isospin T , and T_- is the isospin lower operator. The transition density for this model state is given by $\rho_n(r) - \rho_p(r)$ the difference between the neutron and proton densities. The Coulomb interaction of the protons does affect the distribution of the Z protons in the nucleus and the density distribution of the Z neutrons is different from the distribution of the Z protons. As discussed in the past [1], because of the Coulomb repulsion, the Z protons have a larger radius compared to the corresponding Z neutrons. The Z neutrons and the Z protons are denoted as the core (we assume that we deal with nuclei that $N > Z$). We make the following decomposition:

$$\rho_n(r) - \rho_p(r) = \rho_{n(exc)}(r) + \delta\rho(r), \quad (2)$$

where $\delta\rho(r)$ denotes the density of the Z neutrons of the core minus the density of the protons

$$\delta\rho(r) = \sum_{i=1}^Z |\varphi_i^n(r)|^2 - \sum_{i=1}^Z |\varphi_i^p(r)|^2 \quad (3)$$

and $\rho_{n(exc)}$ the density of $N - Z$ excess neutrons

$$\rho_{n(exc)}(r) = \sum_{i=Z+1}^N |\varphi_i^n(r)|^2, \quad (4)$$

with $\varphi_i^{n(p)}(r)$ being the neutron (proton) single-particle wave function. The volume integral of $\delta\rho(r)$ must be zero and therefore this term must have at least one node. The inside part is positive while the surface part is negative because there is an excess of protons outside, since the protons are expelled by the Coulomb interaction. The $\delta\rho(r)$ term was studied in the past and it was shown that the shape of this distribution can be approximated by the relation [1]:

$$\delta\rho(r) \sim \left(3\rho(r) + r \frac{d\rho(r)}{dr} \right), \quad (5)$$

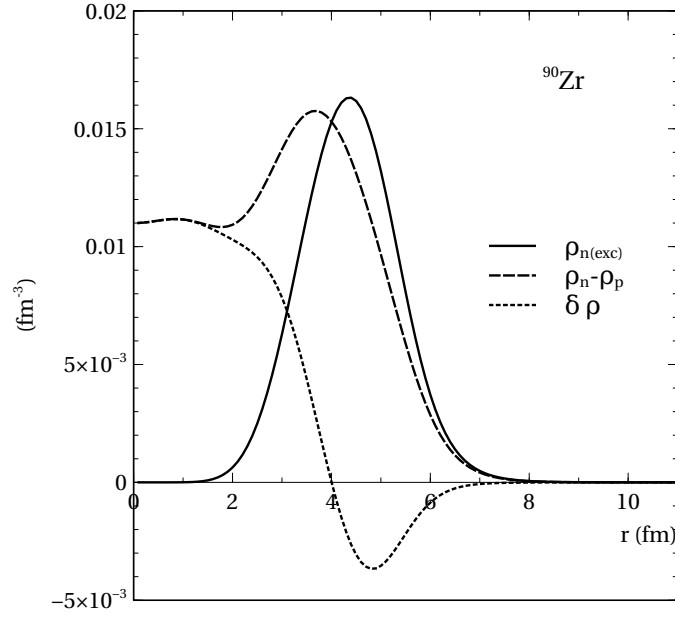


FIG. 1. $\rho_n(r) - \rho_p(r)$, $\rho_{n(exc)}(r)$, and $\delta\rho(r)$ of the ^{90}Zr nucleus obtained from the HF-BCS calculation using the BSk17 version of Skyrme interaction.

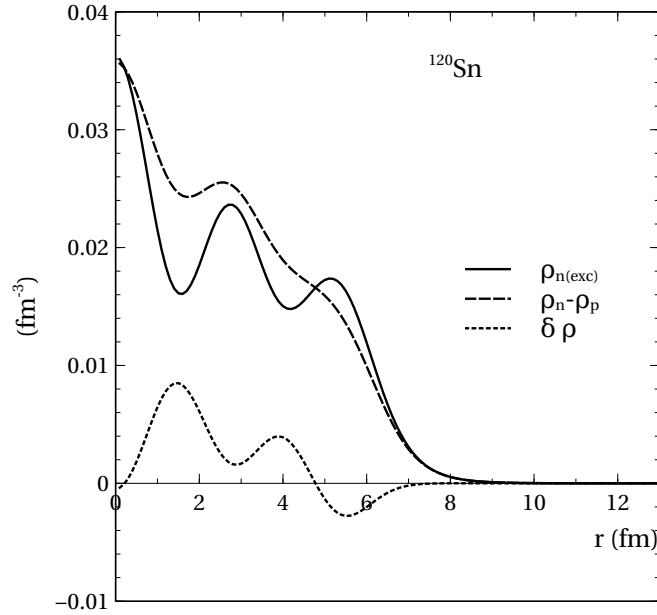


FIG. 2. The same as in Fig. 1, but for ^{120}Sn nucleus.

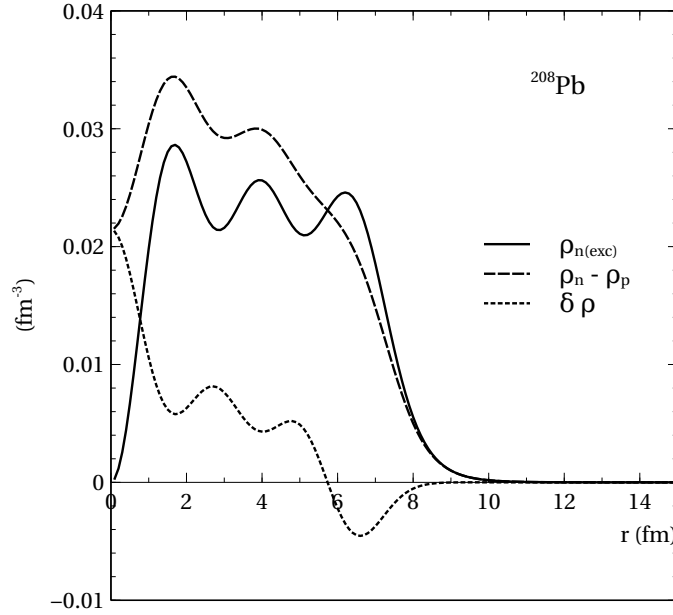


FIG. 3. The same as in Fig. 1, but for ^{208}Pb nucleus.

where $\rho(r)$ is the total nuclear density.

When a projectile probes the interior of the nucleus it will experience the interior transition density as well as the exterior one. These are of opposite signs in $\delta\rho(r)$ and therefore there *should not be much difference between the use of $\rho_n(r) - \rho_p(r)$ or $\rho_{n(exc)}(r)$* . This changes when the projectile reaches the surface but does not penetrate the interior. In this case the projectile will experience the excess neutron density and the external part of $\delta\rho(r)$. This really means the projectile experience somewhat less neutrons at the surface compared to the case when only excess neutrons are present. Thus the two transition densities will *give different results for the SCX cross-sections to the IAS*. The transition will be, therefore, larger when the excess neutron density is used. In the past this picture was shown to be valid for pion SCX reactions were used. We are still left with the question, which of the two transition densities should be used in the SCX to the IAS. This question was answered in the past in several references [2, 3].

If one uses the definition of the IAS, Eq. (1), then $\rho_n(r) - \rho_p(r)$ is the correct one. But this is not the physical analog state. It was shown in [2, 3] that due to the Coulomb interaction the physical state is such that the $\rho_{n(exc)}$ is the proper transition density. When the T_-

operator acts on all neutrons it also affects the core neutrons because the corresponding proton orbits are slightly different from the neutron orbits and thus the Pauli principle allows partially to change the neutron wave functions when the T_- operator acts. However the physical IAS does not have the core affected. ^{41}Ca ground state and its IAS, that is the ground state of ^{41}Sc have the same cores, only the last neutron, with a neutron wave function is transformed into a proton in the same orbit but with a proton wave function. A correct description of this is to use the *analog spin scheme* [2, 4] in which the W_- operator changes a neutron with a neutron wave function into a proton in the same orbit but with the proton wave function.

In the recent years, new SCX to the IAS experiments were performed using light ions, in particular the $(^3\text{He}, t)$ reaction. Also the theoretical analysis of these reactions have been presented [5].

II. METHOD OF CALCULATION

The method of calculation to obtain the differential cross-section in this work is as same as Ref. [5]. The SCX to the IAS is described within the distorted wave Born approximation (DWBA). The phenomenological optical parameters of the ^3He scattering from ^{58}Ni and ^{90}Zr are taken from Ref. [6]. For ^{208}Pb target, the parameters are taken from the optical model fit [7] of the elastic ^3He scattering data at 450 MeV [8]. The SCX form factor is given by the double-folding model (DFM) in the following form

$$F_{\text{cx}}(R) = \sqrt{\frac{2}{T}} \iint [\rho_n^a(\mathbf{r}_a) - \rho_p^a(\mathbf{r}_a)] t_{01}(E, s) [\rho_n^A(\mathbf{r}_A) - \rho_p^A(\mathbf{r}_A)] d\mathbf{r}_a d\mathbf{r}_A, \quad (6)$$

where s is the relative coordinate between a nucleon in projectile and a nucleon in the target. The nucleon-nucleon effective interaction $t_{01}(E, s)$ in Eq. (6) is the Franey-Love t -matrix [9, 10]. The neutron and proton densities of ^3He are given by the microscopic three-body calculation [11] using the Argonne nucleon-nucleon potential. The calculations of the densities and radii of target nuclei are performed using the Hartree-Fock (HF) [12] or in cases of open shell nuclei using HF-BCS approximations [13] with Skyrme type interactions. The BSk17 parametrization [14] was employed. The details of folding model calculation for SCX reaction to the IAS was given in Ref. [15]. The DWBA calculations were done with the relativistic kinematics, using the code ECIS06 written by Raynal [16].

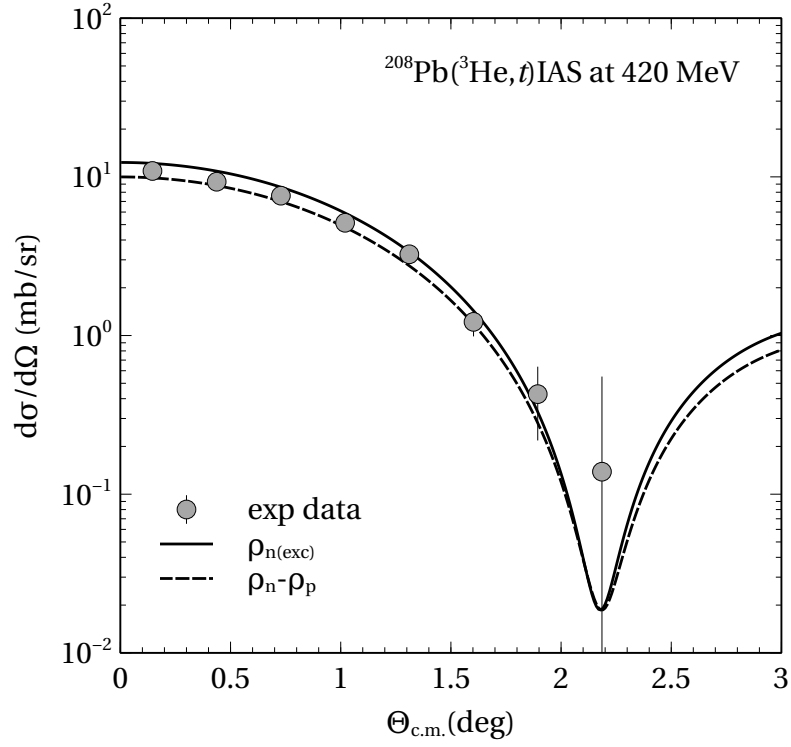


FIG. 4. Differential cross section of the $^{208}\text{Pb}(^3\text{He}, t)$ reaction to the IAS at $E_{\text{lab}} = 420$ MeV, given by the DWBA calculation using the SCX form factors obtained with the $\rho_n(r) - \rho_p(r)$ (dashed curve) and the $\rho_{n(\text{exc})}(r)$ (solid curve). The experimental data were taken from Ref. [7].

TABLE I. Properties of nuclear densities calculated using the Skyrme HF-BCS calculation.

| | ^{58}Ni | ^{90}Zr | ^{120}Sn | ^{208}Pb |
|--------------------------------------|------------------|------------------|-------------------|-------------------|
| $(N - Z)/A$ | 0.034 | 0.111 | 0.167 | 0.212 |
| r_n | 3.691 | 4.267 | 4.706 | 5.594 |
| r_p | 3.694 | 4.202 | 4.573 | 5.441 |
| $r_n - r_p$ | -0.003 | 0.065 | 0.133 | 0.153 |
| $(r_n - r_p)_{\text{core}}$ | -0.047 | -0.103 | -0.070 | -0.130 |
| $r_{n(\text{exc})}$ | 4.249 | 4.882 | 5.174 | 6.086 |
| $S_{\delta\rho(\text{sur})}$ | -0.531 | -1.691 | -1.453 | -3.683 |
| $S_{\delta\rho(\text{sur})}/(N - Z)$ | -0.258 | -0.169 | -0.072 | -0.083 |

III. RESULTS AND DISCUSSION

In describing the results we do it in two steps. First we present the results of the structure calculations as these are the input in the reaction computations. In the second step we show the cross section for the two reactions (${}^3\text{He}, t$) and (p, n).

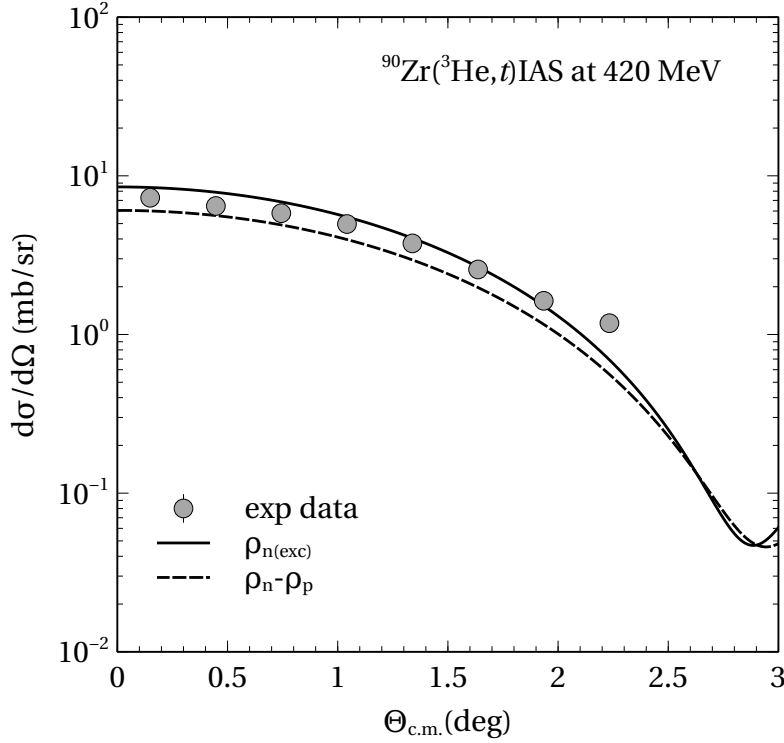


FIG. 5. The same as in Fig. 4, but for ${}^{90}\text{Zr}$ target.

The calculated densities $\rho_n(r) - \rho_p(r)$, $\rho_{n(\text{exc})}(r)$, and $\delta\rho(r)$ for several nuclei are shown in Fig. 1, 2, and 3. The curve of $\rho_n(r) - \rho_p(r)$ is the sum of $\rho_{n(\text{exc})}(r)$ and $\delta\rho(r)$. One sees that $\delta\rho(r)$ has a node and the inner region is positive meaning that there are more neutrons than protons in the $N = Z$ core but in the outer region the density is negative, thus there is a surplus of protons, due to the Coulomb repulsion. It is clear that when one uses the $\rho_n(r) - \rho_p(r)$ transition density one has less neutrons at the surface then in the case when the transition density is $\rho_{n(\text{exc})}(r)$. The effect will be the largest when there are fewer excess neutrons in the nucleus as is the case of ${}^{58}\text{Ni}$. This will affect the SCX reactions when the projectiles are absorbed more strongly and do not reach the interior, in particular ion projectiles such as ${}^3\text{He}$. When a projectile traverses the entire (or most) of the nucleus

this effect of Coulomb polarization density $\delta\rho(r)$ will be small. One should expect therefore that in (p, n) reactions the effect of $\delta\rho(r)$ will be less pronounced to that of $(^3\text{He}, t)$ reaction (of course this also depends on the energies of the projectiles, as for different energies the absorption might be different). In the past it was pointed out [17, 18] and also confirmed experimentally [19] that projectiles that are strongly absorbed will excite states that have radial transition densities consisting of a volume and surface parts of opposite sign, as for example the giant monopole or spin monopole [17–19].

In Table I some of the properties of the densities and radii of nuclei in the study are summarized. The meaning of various quantities appearing in the table is obvious except $S_{\delta\rho(sur)}$ which denotes the integral of $\delta\rho(r)$ from its last node R_s of the density to infinity,

$$S_{\delta\rho(sur)} = 4\pi \int_{R_s}^{\infty} [(\rho_n(r) - \rho_p(r)) - \rho_{n(exc)}(r)] r^2 dr. \quad (7)$$

This is an illustrative, approximate way to quantify the amount of protons that are at the surface due to the Coulomb polarization of the Z protons in the core. As already mentioned the effect of $\delta\rho(r)$ is largest when the number of excess neutrons is small. Note that in ^{58}Ni the difference $r_n - r_p$ is actually negative. This is in agreement with the prediction in Ref. [20] and the difference $(r_n - r_p)_{core}$ is in reasonable agreement with the formula derived in the Ref. [20]

$$(r_n - r_p)_{core} = -1.6 \times 10^{-3} Z. \quad (8)$$

So what effect do the above density distribution have on the SCX cross-section? We now discuss the results of the DWBA calculations. The structure ingredients discussed above are tested in our analysis of the $(^3\text{He}, t)\text{IAS}$. In Fig. 4 the $(^3\text{He}, t)$ differential cross-sections at 420 MeV are shown for ^{208}Pb using the transition densities $\rho_n(r) - \rho_p(r)$ and $\rho_{n(exc)}$. We see that the cross-section calculated with $\rho_{n(exc)}(r)$ is slightly higher than with $\rho_n(r) - \rho_p(r)$ but the difference is not large, consistent with the fact that the number of protons pushed out by the Coulomb force is large (about 4) but compared to the 44 excess neutrons the effect is small.

In Fig. 5 the same results are plotted for ^{90}Zr but in this case due to the smaller number of excess neutrons the effect is larger. The cross-section with $\rho_{n(exc)}(r)$ is larger and closer to the experimental results [7]. The results for ^{58}Ni are shown in Figure 6. Here the number of excess neutrons is 2, and the effect of $\delta\rho_{sur}$ compared to $\rho_{n(exc)}$ is sizable (see Table I).

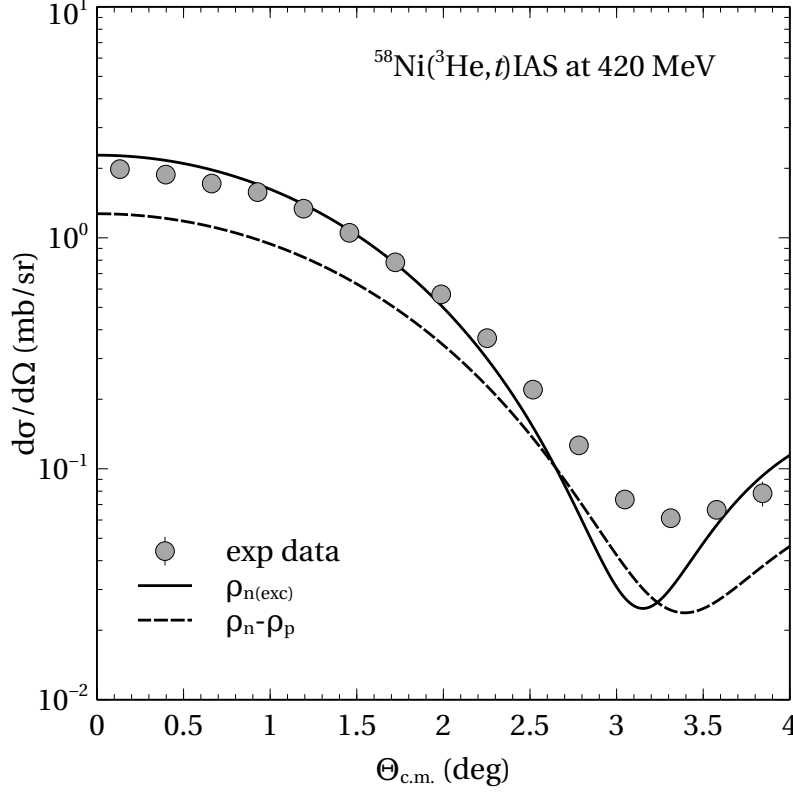


FIG. 6. The same as in Fig. 4, but for ^{58}Ni target.

The cross-section in the forward direction is increased by more than a factor of 2, agreeing with the experimental data.

It is interesting to contrast the $(^3\text{He},t)$ IAS reaction with the (p,n) IAS reaction. As mentioned above the latter one (depending on the energy) may probe the interior of the nucleus and would be less sensitive to the polarization of the core. The results of the calculations using the two transition densities should be close. In Fig. 7, we show the prediction for the $^{120}\text{Sn}(p,n)$ IAS reaction at 170 MeV for the two transition densities. Here the difference between the two curves is very small.

IV. CONCLUSIONS

We discussed in the present work the impact of two forms of transition densities used in the charge-exchange reactions to the IAS. We found that when the projectile used in the reaction does not probe the interior of the nucleus but mostly the surface, visible difference in the cross-sections arise when the two densities are employed. The $(^3\text{He},t)$ IAS reaction at

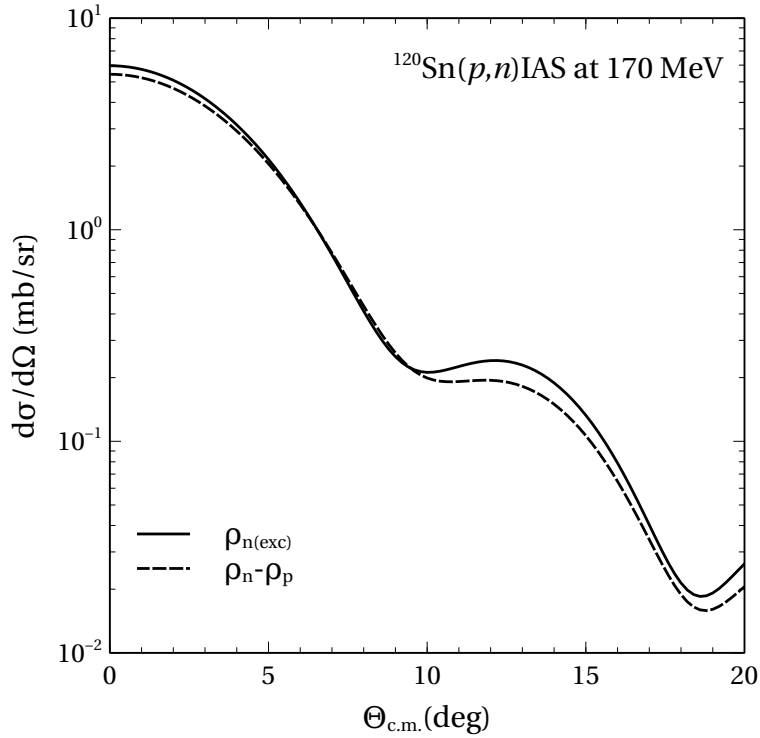


FIG. 7. Differential cross sections of the $^{120}\text{Sn}(p,n)\text{IAS}$ reaction at $E_{\text{lab}} = 170$ MeV, given by the DWBA calculation using the SCX form factors obtained with $\rho_n(r) - \rho_p(r)$ (dashed curve) and the $\rho_{n(\text{exc})}(r)$ (solid curve).

medium energies is of this type and in nuclei with a low number of excess neutrons this effect is enhanced. Single charge-exchange, and double charge-exchange reactions with complex projectiles may provide useful tools to study the neutron-proton content at the surface of the nucleus.

ACKNOWLEDGMENTS

The authors thank to Gianluca Colò for providing us with the HF-BCS code. This work was supported, in part, by the US-Israel Binational Science Foundation (grant 2014.24) and Vietnam's National Foundation for Science and Technology Development (NAFOSTED

project No. 103.04-2014.76).

- [1] N. Auerbach, Phys. Rep. **98**, 273 (1983).
- [2] N. Auerbach and N. Van Giai, Phys. Rev. C **24**, 782 (1981).
- [3] N. Auerbach and A. Yeverechyahu, Phys. Rev. C **25**, 2841 (1982).
- [4] A. Mekjian and W. Macdonald, Nucl. Phys. A **121**, 385 (1968).
- [5] B. M. Loc, D. T. Khoa, and R. G. T. Zegers, Phys. Rev. C **89**, 024317 (2014).
- [6] J. Kamiya, et al., Phys. Rev. C **67**, 064612 (2003).
- [7] R. G. T. Zegers, et al., Phys. Rev. Lett. **99**, 202501 (2007).
- [8] T. Yamagata, et al., Nucl. Phys. A **589**, 425 (1995).
- [9] W. G. Love and M. A. Franey, Phys. Rev. C **24**, 1073 (1981).
- [10] M. A. Franey and W. G. Love, Phys. Rev. C **31**, 488 (1985).
- [11] E. Nielsen, D. Fedorov, A. Jensen, and E. Garrido, Phys. Rep. **347**, 373 (2001).
- [12] G. Colò, L. Cao, N. V. Giai, and L. Capelli, Comput. Phys. Commun. **184**, 142 (2013).
- [13] G. Colò, private communication (unpublished).
- [14] S. Goriely, N. Chamel, and J. M. Pearson, Phys. Rev. Lett. **102**, 152503 (2009).
- [15] D. T. Khoa., B. M. Loc, and D. N. Thang, Eur. Phys. J. A **50**, 1 (2014).
- [16] J. Raynal, Coupled-Channels code ECIS06 (<https://www-nds.iaea.org/RIPL-3/>, 2006).
- [17] N. Auerbach, Comments Nucl. Part. Phys. **32** (1998).
- [18] N. Auerbach, F. Osterfeld, and T. Udagawa, Phys. Lett. B **219**, 184 (1989).
- [19] D. L. Prout, et al., Phys. Rev. C **63**, 014603 (2000).
- [20] N. Auerbach, Phys. Rev. C **81**, 067305 (2010).